Van Allen Probes observations of prompt MeV radiation belt electron acceleration in nonlinear interactions with VLF chorus

Citation: Foster, J. C., P. J. Erickson, Y. Omura, D. N. Baker, C. A. Kletzing, and S. G. Claudepierre. "Van Allen Probes Observations of Prompt MeV Radiation Belt Electron Acceleration in Nonlinear Interactions with VLF Chorus." Journal of Geophysical Research: Space Physics 122, no. 1 (January 2017): 324–339.

As Published: http://dx.doi.org/10.1002/2016JA023429

Publisher: American Geophysical Union (AGU)

Persistent URL: http://hdl.handle.net/1721.1/110600

Version: Final published version: final published article, as it appeared in a journal, conference proceedings, or other formally published context

AGU PUBLICATIONS

JGR

Journal of Geophysical Research: Space Physics

RESEARCH ARTICLE
10.1002/2016JA023429

Key Points:
- Prompt (<1 h) MeV electron acceleration in the inner magnetosphere accompanies substorm injections and strong VLF chorus rising tones
- Highly coherent subpacket structure in strong VLF rising tones accounts for significant nonlinear acceleration efficiency
- MeV seed electrons can be accelerated by 50 keV–200 keV in 10–100 ms in nonlinear interactions with a single VLF chorus rising tone

Correspondence to:
J. C. Foster,
jfoster@haystack.mit.edu

Citation:
Foster, J. C., P. J. Erickson, Y. Omura, D. N. Baker, C. A. Kletzing, and S. G. Claudepierre (2016), Van Allen Probes observations of prompt MeV radiation belt electron acceleration in nonlinear interactions with VLF chorus, *J. Geophys. Res. Space Physics*, *122*, doi:10.1002/2016JA023429.

Received 2 SEP 2016
Accepted 29 DEC 2016
Accepted article online 31 DEC 2016

Van Allen Probes observations of prompt MeV radiation belt electron acceleration in nonlinear interactions with VLF chorus

J. C. Foster[1], P. J. Erickson[1], Y. Omura[2], D. N. Baker[3], C. A. Kletzing[4], and S. G. Claudepierre[5]

[1]Haystack Observatory, Massachusetts Institute of Technology, Westford, Massachusetts, USA, [2]Research Institute for Sustainable Humanosphere, Kyoto University, Kyoto, Japan, [3]Laboratory for Atmospheric and Space Physics, University of Colorado, Boulder, Boulder, Colorado, USA, [4]Department of Physics and Astronomy, University of Iowa, Iowa City, Iowa, USA, [5]Aerospace Corporation, Los Angeles, California, USA

Abstract Prompt recovery of MeV (millions of electron Volts) electron populations in the poststorm core of the outer terrestrial radiation belt involves local acceleration of a seed population of energetic electrons in interactions with VLF chorus waves. Electron interactions during the generation of VLF rising tones are strongly nonlinear, such that a fraction of the relativistic electrons at resonant energies are trapped by waves, leading to significant nonadiabatic energy exchange. Through detailed examination of VLF chorus and electron fluxes observed by Van Allen Probes, we investigate the efficiency of nonlinear processes for acceleration of electrons to MeV energies. We find through subpacket analysis of chorus waveforms that electrons with initial energy of hundreds of keV to 3 MeV can be accelerated by 50 keV–200 keV in resonant interactions with a single VLF rising tone on a time scale of 10–100 ms.

1. Introduction

The characteristics and dynamics of ultrarelativistic MeV (millions of electron Volts) electron fluxes in Earth's outer radiation belt are strongly influenced by geomagnetic storm time processes, leading both to significant electron loss and local acceleration deep within the inner magnetosphere [*Ukhorskiy et al.*, 2014; *Reeves et al.*, 2013]. *Thorne et al.* [2013], modeling radiation belt recovery during an October 2012 storm, identified acceleration by VLF (very low frequency) chorus during low-energy electron injections as responsible for local MeV acceleration in the heart of the radiation belt. Using Van Allen Probes spacecraft observations near apogee (~5.5 R_E), *Foster et al.* [2014] described observations of electron injection and chorus amplification associated with a substorm dipolarization during the 17 March 2013 storm. Subsequent recovery of the MeV electron population was observed within ~1 to 4 h at varying radial distances in the outer electron belt.

In this study, we investigate the energization of highly relativistic (1–5 MeV) electrons in the core of the storm-depleted outer radiation belt using observations from the twin Van Allen Probes satellites (also known as the Radiation Belt Storm Probes, RBSP) [*Mauk et al.*, 2013]. These are combined with theory and modeling by *Omura et al.* [2015] that describe the effective acceleration of energetic electrons by relativistic turning acceleration (RTA) [*Omura et al.*, 2007] and ultrarelativistic acceleration (URA) [*Summers and Omura*, 2007] processes through nonlinear trapping by chorus emissions. During the 17 March 2013 storm, the Van Allen Probes A and B spacecraft crossed the inner portions of the outer electron radiation belt with ~1 h time separation along the same spatial orbital trajectory at the time of a substorm injection. They were therefore well situated to observe directly the characteristics and effects of local acceleration through quantification of conditions before and after energization took place. We find that evidence for nonlinear acceleration processes, and for rapid (<1 h) energization of seed electrons to MeV energies, is associated with injections of tens of keV to hundreds of keV electrons into the inner magnetosphere during substorms.

During times of outer belt chorus enhancement, lower energy electrons in the 10 to 80 keV range provide a source of free energy to VLF waves and subsequently are driven into the loss cone, precipitating into the atmosphere [e.g., *Foster and Rosenberg*, 1976]. At the same time, the high-energy tail of the electron distribution gains perpendicular energy from the same waves and is accelerated [*Summers et al.*, 1998; *Albert*, 2002; *Horne et al.*, 2005; *Cattell et al.*, 2008; *Bortnik et al.*, 2008; *Thorne et al.*, 2013; *Brautigam and Albert*, 2000;

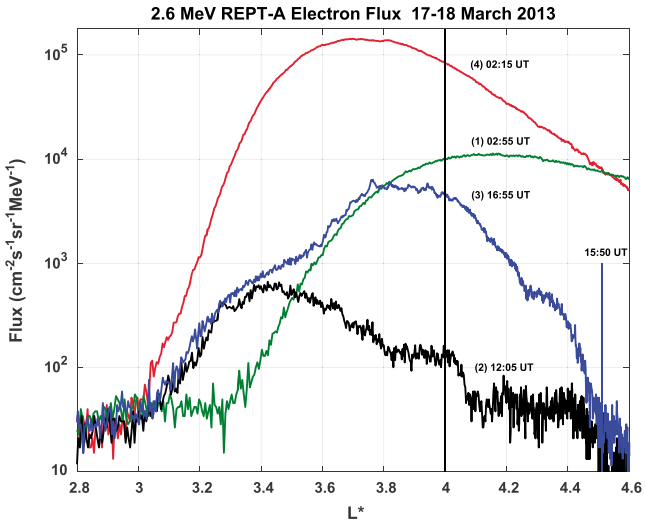

Figure 1. The *L** variation of REPT A 2.6 MeV electron fluxes during the 17–18 March 2013 storm are shown for passes across the outer radiation belt by Van Allen Probe A. Passes are labeled with the time of crossing *L** = 4.0 (vertical black line). The prestorm *L** profile is shown in green (#1 at 2:55 UT). Storm time depletion of the outer belt is shown in black (#2 at 12:05 UT) when 2.6 MeV flux was decreased by a factor of ~100. The blue curve (#3 at 16:55 UT) reflects the effects of the substorm injection at 15:50 UT that resulted in a partial recovery (>10X) of the outer belt relativistic electron flux. A second substorm onset at 22:15 UT was followed by a further ~30X increase in the 2.6 MeV flux (#4 red curve; 02:15 UT on 18 March).

Miyoshi et al., 2003, 2013]. Theoretical investigations [*Omura et al.*, 2008, 2009; *Omura and Nunn*, 2011] and simulations [*Katoh and Omura*, 2007; *Hikishima et al.*, 2009] describe the rapid nonlinear growth of this interaction during the generation of strong VLF rising tones. Following a linear phase of chorus wave amplification, a threshold amplitude is reached where a portion of the high-energy electron population undergoes nonlinear resonant motion forming an electron hole in the velocity phase space, resulting in resonant currents inducing frequency increase and wave growth. The extent of the electron population involved in this nonlinear wave growth increases as events progress, and the rising tone chorus wave amplitude intensifies, due to the expansion of the electron hole [*Omura et al.*, 2012]. A fraction of the resonant electrons are trapped in the hole, and they are accelerated efficiently through nonlinear trapping [*Omura et al.*, 2015].

Section 2 presents an overview of the Van Allen Probes observations associated with the prompt acceleration of outer zone radiation belt relativistic electrons during substorm injection events for the major geomagnetic storm that began on 17 March 2013. Characteristics of the strong VLF chorus rising tones observed at the time of local MeV electron acceleration in the inner magnetosphere are described in section 3. Section 4 describes the application of subpacket wave analysis to individual chorus rising tones in order to address the nonlinear acceleration capacity of chorus emissions in the outer radiation belt during substorm injection events. It is found that resonant seed electrons with initial energies ~1 MeV can gain ~100 keV in a 10–20 ms interaction with a single chorus wave subpacket. Section 5 presents results that demonstrate good consistency between the electron acceleration observations of section 2 and the theoretical analyses of electron acceleration by chorus rising tones presented in section 4.

2. Event Characteristics

Driven by a solar wind shock, the 17 March 2013 event resulted in an extensive dropout of relativistic electron flux across the entire range of the outer belt, reaching inward to $L \sim 3$ [e.g., *Baker et al.*, 2014; *Ukhorskiy et al.*, 2014, 2015]. This was followed by a rapid recovery in energetic relativistic electron fluxes over the course of the next 12–24 h [e.g., *Foster et al.*, 2014]. *Li et al.* [2014] have modeled the recovery of radiation belt electrons over the course of ~24 h by quasi-linear interactions with VLF chorus. That study has presented a detailed picture of interplanetary and magnetospheric parameters for this event. Separately, *Xiao et al.* [2014] investigated local acceleration driven by lower band chorus during this event, concluding that the observed increase in relativistic electron flux can be produced after ~15 h of relatively steady flux increase. Recent studies [e.g., *Boyd et al.*, 2014; *Li et al.*, 2014; *Jaynes et al.*, 2015] have discussed the substorm-associated increase in

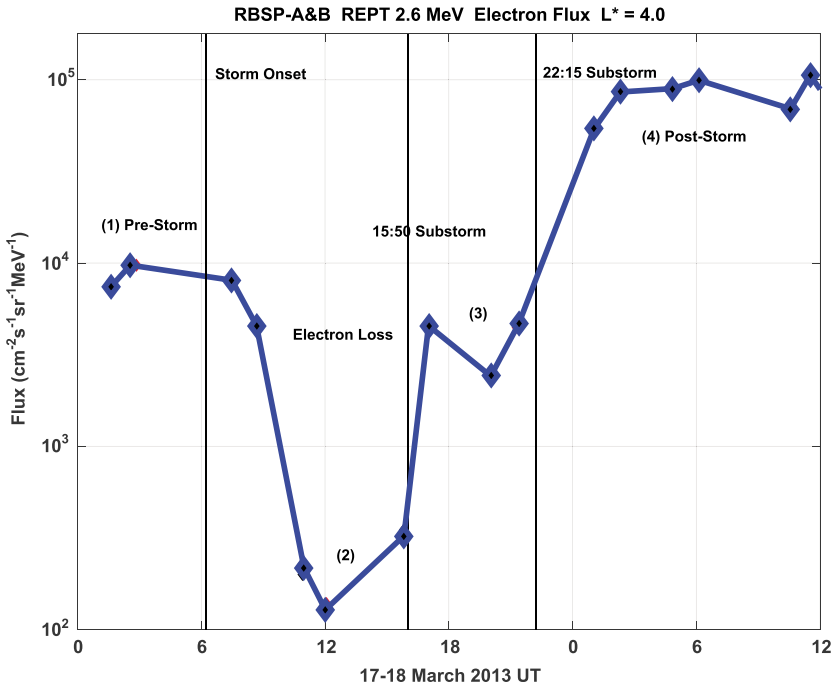

Figure 2. Storm time changes in the 2.6 MeV electron fluxes observed at $L^* = 4.0$ with the REPT instruments on both Van Allen Probes delineate the event time history of relativistic electron loss and recovery. Storm onset was at ~06:15 UT on 17 March 2013 and prompt stepwise radiation belt energization accompanied substorm injections at 15:50 UT and 22:15 UT. Diamonds indicate the sequential observations by Probes A and B at $L^* = 4.0$. Numbers (1–4) refer to the profiles of Figure 1.

the near-relativistic seed electron population as an important factor for the acceleration of electrons to MeV energies. Here we investigate observations associated with the rapid (<1 h) energization of seed electrons to MeV energies at the time of a substorm injection during the 17 March 2013 event.

For four passes across the outer radiation belt, Figure 1 presents observations of 2.6 MeV electron flux measured by the Relativistic Electron-Proton Telescope (REPT) instrument [*Baker et al.*, 2013a] on Van Allen Probes A, plotted against L^* calculated using the TS04D magnetic field model [*Tsyganenko and Sitnov*, 2005]. (L^* [*Roederer and Zhang*, 2014], is directly proportional to the integral of the magnetic flux contained within the surface defined by a charged particle moving in the Earth's geomagnetic field ($\mathbf{B_0}$). Under adiabatic changes to $\mathbf{B_0}$, L^* is a conserved quantity.) The prestorm outer belt is depicted in green for the pass (#1) crossing $L^* = 4.0$ at 02:55 UT. The extent of the depleted outer belt at the height of the storm is seen in the 12:05 UT pass (#2) shown in black. Following a substorm with onset at ~15:50 UT, a partial recovery (~10X) of the outer belt relativistic electron flux was observed (blue curve (#3) at 16:55 UT). A second substorm injection followed at ~22:15 UT. During the following inbound pass (red curve #4 at 02:15 UT on 18 March) a further recovery (30*x*) of the energetic relativistic electron fluxes across the full extent of the outer belt was observed. (See *Foster et al.* [2014], for further discussion of the 22:15 UT substorm event.)

Figure 2 presents an overview of the storm time changes in relativistic electron flux in the core of the outer radiation belt for the 17–18 March 2013 event. The blue curve plots the time history of REPT observations of 2.6 MeV electron flux at $L^* = 4.0$ through the event (diamonds indicate the individual observations by Probes A and B at $L^* = 4.0$). Vertical lines are drawn denoting the times of storm and substorm onsets. A 100X flux decrease was observed in the initial phases of the storm. (*Ukhorskiy et al.* [2014] discuss radiation belt losses to the magnetopause during this event.) A sharp >10X recovery was observed in a ≤1 h interval associated with the 15:50 UT substorm, and a further 30X flux increase at 2.6 MeV was observed in the ≤4 h observation interval following the 22:15 UT substorm. The time intervals ascribed to the local acceleration during these substorm events are determined by the time differences of successive inner magnetosphere passes across $L^* = 4.0$ by either of the two Van Allen Probes.

As described previously, the local acceleration of relativistic electrons involves the injection of low-energy electrons, VLF chorus wave enhancement, and the presence of a population of energetic seed electrons

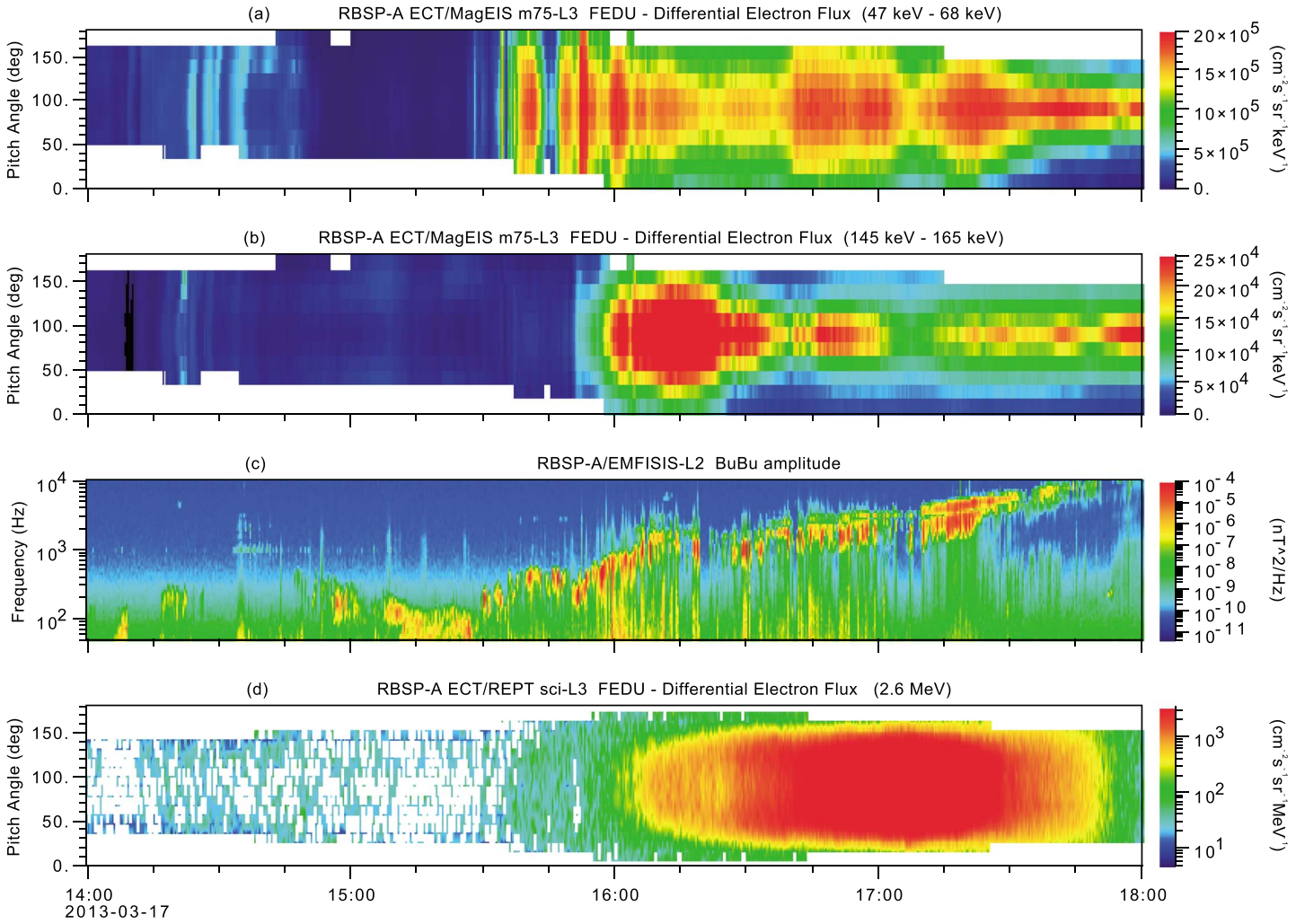

Figure 3. Local acceleration involves the enhancement of VLF chorus by lower energy injected electrons and the subsequent energization of a seed population of higher-energy electrons by the amplified waves. (a) RBSP A MagEIS observations of injected ~50 keV and (b) ~150 keV electrons and (c) associated chorus emissions observed by EMFISIS A are shown for the 15:50 UT substorm interval. (d) The growing enhancement of 2.6 MeV electrons resulting from the local acceleration of the near-relativistic seed population.

that can take energy from the waves through resonant interactions, either slowly (quasi-linear diffusion by low-amplitude waves) or quickly (nonlinear effects at high amplitudes). For the substorm with onset at ~15:50 UT on 17 March 2013, Figure 3 presents Van Allen Probe A observations of injected ~50 keV and 150 keV electrons in Figures 3a and 3b (measured with the Magnetic Electron Ion Spectrometer (MagEIS) instrument [*Blake et al.*, 2013]). In situ electric fields were observed by the electric field and waves instrument [*Wygant et al.*, 2013] on RBSP A during the substorm (not shown). These electric fields were not of sufficient magnitude to contribute to the direct energization of electrons to MeV energies but can account for the observed injected electron fluxes with energy below ~250 keV. Thus, abundant pump electrons were available to drive chorus wave growth in the inner magnetosphere outside the plasmapause. The related VLF chorus enhancement observed with the Electric and Magnetic Field Instrument Suite and Integrated Science (EMFISIS) [*Kletzing et al.*, 2013] is shown in Figure 3c. Low-energy injected electrons and enhanced chorus emissions were observed for more than an hour following substorm onset. The REPT instruments on both RBSP A and B spacecraft made simultaneous observations of MeV electron flux with good energy and pitch angle resolution [*Baker et al.*, 2013a, 2013b]. Figure 3d shows the prompt enhancement of 2.6 MeV electron flux observed by REPT A consistent with the local acceleration of a near-relativistic population of seed electrons. Adiabatic changes in the energetic electron fluxes due to magnetic field compression and relaxation during the substorm depolarization events at both 15:50 UT and 22:15 UT were confined to the initial ~30 min of each

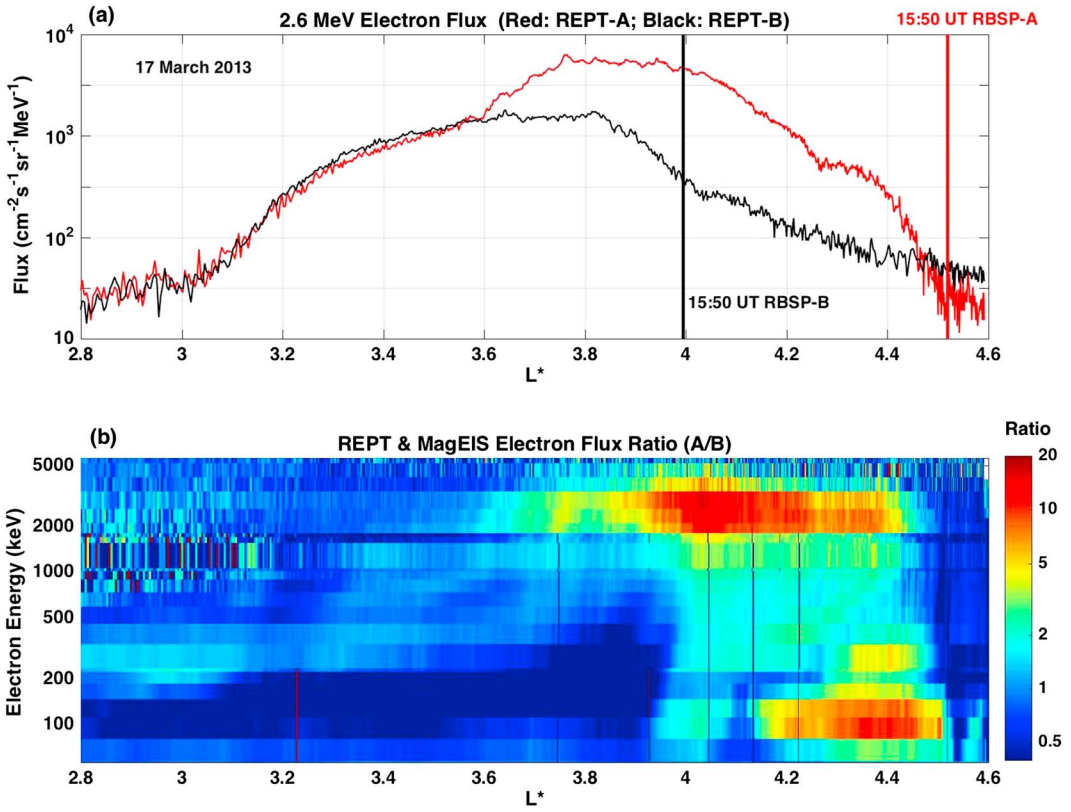

Figure 4. (a) Sequential profiles of 2.6 MeV electron flux measured by the dual Van Allen Probes are shown. During the event, RBSP A followed RBSP B by ~1 h along the same orbital trajectory. RBSP B was at L^* ~ 4.0 at the 15:50 UT substorm onset, while RBSP A was at L^* ~ 4.5. On its inbound orbit RBSP B observed presubstorm background fluxes over L^* ~ 4.5–4.0, while RBSP A observed postsubstorm enhancements. The plasmapause was observed at L^* ~ 2.5 at 17:10 UT. (b) Ratios of electron flux (RBSP A (post substorm)/RBSP B (presubstorm)) are shown up to ultrarelativistic energies using MagEIS and REPT combined data (REPT data ≥ 1.8 MeV). Injected ~50–150 keV electrons were seen at RBSP A between L^* ~ 4.5 and 4.1. The prompt onset of strong (> 10*x*) enhancements of ~1–3 MeV electron flux characterize the effects of local acceleration processes during the event.

event. Long duration and spatially widespread <10X flux increases at MeV electron energies were observed thereafter (cf. Figure 2 and *Foster et al.* [2014]).

During the 17 March 2013 storm, the two Van Allen Probes spacecraft traveled nearly identical orbital paths with ~1 h separation. Probe B crossed $L^* = 4.1$ at 15:40 UT (10 min before substorm onset) and Probe A at 16:45 UT (55 min after substorm onset). In this configuration, Probe B sampled the background (presubstorm) outer zone electron fluxes between L^* ~ 4.5 and L^* ~ 4.0, while Probe A measured the post-onset flux enhancement across this span of L^* space. Sequential profiles of 2.6 MeV electron flux measured by the dual Van Allen Probes are shown in Figure 4a. The ratios of electron flux at energies observed by the MagEIS and REPT instruments (ratio = Flux A/Flux B) are shown in Figure 4b on a log scale. The elevated flux ratios between 50 and 150 keV mark the appearance at the RBSP A location of the injected electrons responsible for VLF chorus amplification (cf. Figure 3). A stronger (10X) flux enhancement at 1–3 MeV identifies the effect of local acceleration. The MeV flux increase spans the L^* range over which substorm effects were observed by Probe A, while Probe B observed the presubstorm background. A ~10X enhancement of 2.6 MeV fluxes over the background level was reached within ~30 min of substorm injection onset, indicative of the time scale for local acceleration of radiation belt electrons to highly relativistic energies in such circumstances. The very large (tenfold) observed increase of 2.6 MeV electron flux over <1 h provides a strong indication of the probable importance of nonlinear processes. The observed 10X enhancement significantly exceeds the factor of 2 increase over the same interval obtained through quasi-linear diffusive acceleration (e.g., as shown in the simulations of *Li et al.* [2014]). As we will show below, prompt electron acceleration peaking in the observed 1–3 MeV energy range is consistent with nonlinear interactions with the rising tone VLF chorus elements seen during the event.

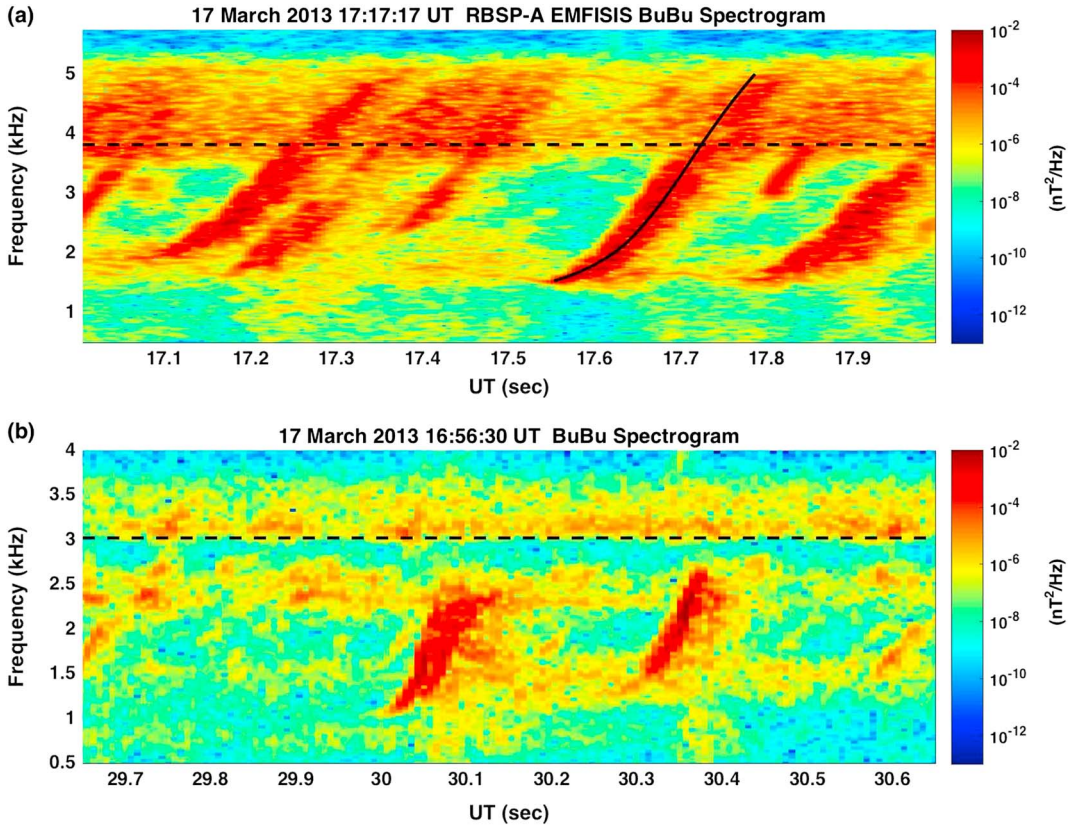

Figure 5. (a) Single-axis (BuBu) magnetic field spectrogram for strong VLF rising tones near 17:17 UT on 17 March 2013 is shown. Each panel shows the fast Fourier transform of ~1 s of burst mode wave observations. The black line superimposed on the 17:17 UT riser shows the optimal values for frequency and frequency sweep rate for a chorus element calculated from nonlinear chorus generation theory (see text). (b) Rising tones near 16:56:30 UT during the same event also have been selected for detailed analysis. On both panels the dashed line indicates $\frac{1}{2}f_{ce}$.

The rapid increase in MeV electron fluxes associated with the 15:50 UT substorm suggests that nonlinear processes play a significant role in the local acceleration of radiation belt electrons in such events. The focus of the current study is to provide an observation-based quantitative assessment of the efficiency of nonlinear RTA and URA processes in accelerating seed electrons to MeV energies. We use dual-satellite Van Allen Probes observations of electron populations and VLF waves during the 17 March 2013 storm to investigate the characteristics of rapid MeV electron energization accompanying substorm injections.

3. VLF Chorus Analysis

Three-axis burst mode EMFISIS observations of wave electric and magnetic fields (28.6 μs time resolution; ~12 kHz maximum observable frequency) are used to investigate electron interactions with individual chorus rising tones on a submillisecond time scale. Strong chorus risers were observed throughout the event. We have selected rising tones at 17:17:17.65 UT and 16:56:30 UT from RBSP A data for detailed analysis. In Figure 5, single-axis (BuBu) magnetic field spectrograms are shown (each panel shows a ~1 s observation). The black line superimposed on the 17:17:17 UT riser shows the optimal values for frequency and frequency sweep rate, calculated from the observed values of electron cyclotron and plasma frequencies using nonlinear chorus generation theory [*Omura et al.*, 2012] (see below). For the rising tone marked with the solid black line in Figure 5a, Van Allen Probes in situ measurements from other spacecraft instruments find $N_e \sim 10\ \mathrm{cm}^{-3}$, $\omega_{pe}/2\pi \sim 30$ kHz, $|\mathbf{B_0}| \sim 270$ nT, and $f_{ce} = \Omega_e/2\pi \sim 7.6$ kHz. Near half the cyclotron frequency ($\frac{1}{2}f_{ce}$; black dashed horizontal line), the wave amplitude undergoes nonlinear wave damping associated with quasi-parallel propagation [*Omura et al.*, 2009].

Based on the dynamic spectrum of the chorus emission, we can estimate the parameters of the energetic electrons generating the emission. Noting that the chorus emission starts from 2 kHz, we iteratively calculate

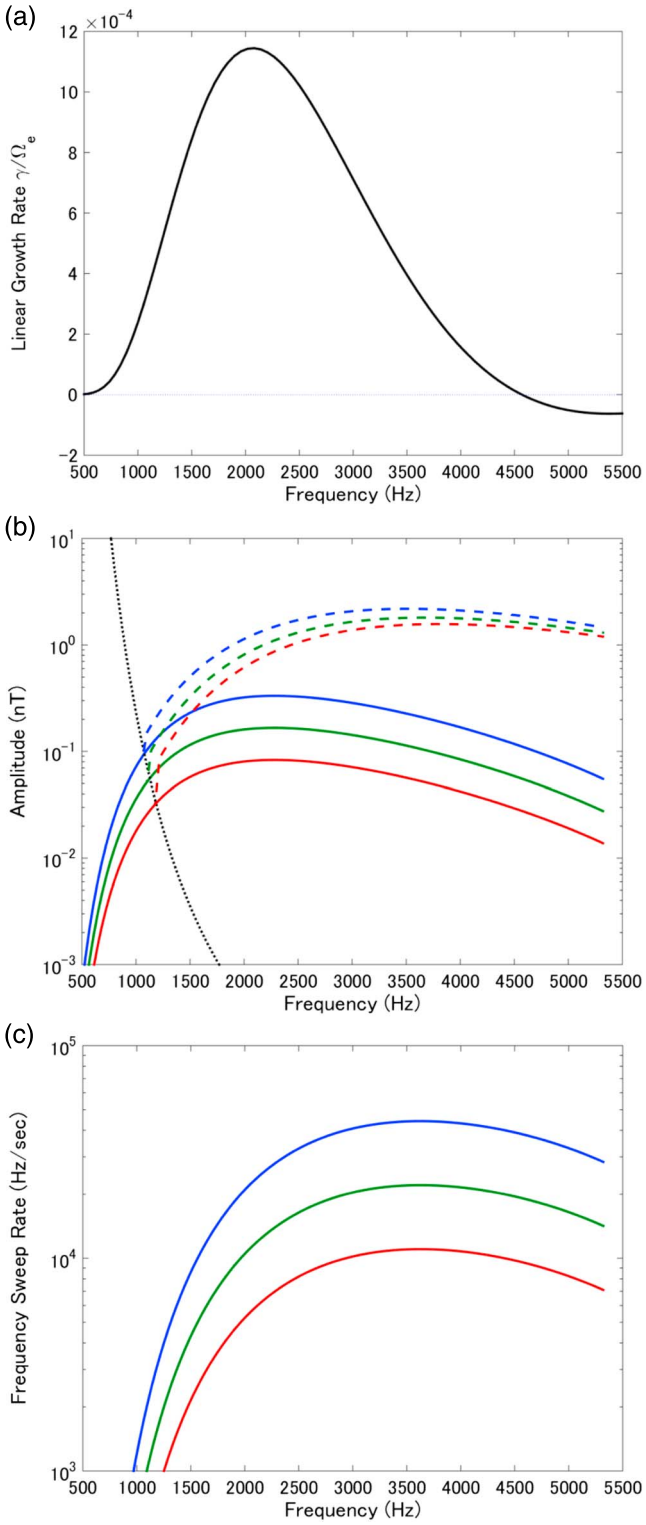

Figure 6. (a) Theoretical linear growth rate, normalized by electron cyclotron frequency, as predicted by KUPDAP for $Vt_{\|} = 0.2c$ and $Vt_{\perp} = 0.32c$. (b) Chorus wave amplitude based on the nonlinear wave growth theory. Plotted are the threshold wave amplitude in nT (black dotted curve), the optimum wave amplitude (solid line), and the amplitude after convective growth (dashed line) for nonlinear transition to trapping time ratios $\tau = 0.25$ (blue), 0.5 (green), and 1.0 (red). (c) The theoretical frequency sweep rates from the optimum wave amplitudes are shown for the same range of τ.

the parallel and perpendicular thermal velocities ($Vt_{\parallel}$ and $Vt_{\perp}$) of an assumed bi-Maxwellian distribution for the energetic electrons that produce maximum linear growth rates of the whistler mode wave at 2 kHz. Using the Kyoto University Plasma Dispersion Analysis Package (KUPDAP) [*Sugiyama et al.*, 2015], we obtain the linear growth rate shown in Figure 6a with $Vt_{\parallel} = 0.2c$ and $Vt_{\perp} = 0.32c$. This value of $Vt_{\perp}$ gives an average perpendicular velocity for electrons responsible for wave growth as $V_{\perp 0} = 0.4c$ (corresponding to ~50 keV electrons). We show in Figure 6b the optimum and threshold amplitudes for nonlinear wave growth calculated for different values of $\tau = 0.25$, 0.5, and 1.0, where τ is the ratio of nonlinear transition time to nonlinear trapping time [*Omura and Nunn*, 2011]. For the curvature of the background magnetic field, we assume a dipole magnetic field with $L = 4.4$.

The optimum wave amplitude, which determines the frequency sweep rate, is controlled by the density n_h of energetic electrons. From the observed sweep rate, we determine the density n_h as 0.03 n_c, where n_c is the cold electron density. Figure 6c shows the frequency sweep rates corresponding to the optimum amplitudes shown in Figure 6b. Integrating the frequency sweep rate plotted in green ($\tau = 0.5$), we obtain the frequency variation with time plotted in black over the 17:17:17.65 UT chorus element in Figure 5a. We note the close correspondence between the modeled and the observed frequency variation. The observed frequency sweep at the leading edge of the riser was ~16.5 kHz/s between 2 kHz and 4.5 kHz. The calculated optimum amplitude is smaller than the observed wave amplitude, indicating that the observed chorus wave packet was generated at the equator and propagated some distance along the magnetic field line to the observation point while undergoing substantial convective growth.

Using the nonlinear growth rate Γ_N given by equation (34) of *Omura et al.* [2012] and the wave group velocity, V_g, we integrate Γ_N/V_g over a distance that produces agreement with the observed wave amplitude. The dashed curves in Figure 6b are the resulting amplitude after convective growth and represent wave propagation over 800 km from the equator. The wave-normal angle deviates from the parallel direction (see below), and the estimated amplitude and distance for convective growth can differ from this estimate. However, in the analysis below, we assume quasi-parallel propagation, $\sin^2\theta \ll 1$, where θ is the wave-normal angle [*Omura et al.*, 2009]. This assumption allows us to use the linear dispersion relation in the parallel direction in evaluating the phase velocity V_p, group velocity V_g, and resonance velocity V_r (cf. equations (6), (8), and (9) below).

To correct the wave analysis for spacecraft spin, we first determine both $\mathbf{B}_{\perp}$, the wave magnetic field perpendicular to the local magnetic field, $\mathbf{B}_0$, and a fixed reference unit vector, $\mathbf{r}$, perpendicular to both $\mathbf{B}_0$ and $\mathbf{R}$, the spacecraft position vector. These definitions then allow calculation of

$$\mathbf{B}_{\perp} = \frac{\mathbf{B}_{\mathrm{wave}} \times \mathbf{B}_0}{|\mathbf{B}_0|}, \tag{1}$$

$$\mathbf{r} = \frac{\mathbf{R} \times \mathbf{B}_0}{|\mathbf{R}|\ |\mathbf{B}_0|}. \tag{2}$$

Finally, we calculate B_1, the despun variation of the wave magnetic field perpendicular to $\mathbf{B}_0$:

$$B_1 = \mathbf{B}_{\perp} \cdot \mathbf{r}. \tag{3}$$

The inverse of twice the time difference between successive zero crossings of B_1 gives the instantaneous wave frequency, $f = \omega/2\pi$, used subsequently in the wave analysis calculations. For the 250 ms extent of the rising tone beginning at 17:17:17.5 UT, the magnitude of $\mathbf{B}_{\perp}$ at the zero crossings, the instantaneous wave frequency, and the wave spectrogram are shown in Figure 7. The magnitude of the wave magnetic field at the zero crossings shows a clear modulation that identifies a sequence of wave subpackets, each spanning multiple wave cycles. *Santolík et al.* [2003, 2004] first identified and described such large-amplitude subpacket structure in Cluster observations of chorus waveforms. Each subpacket represents a single cycle of continuous wave growth and damping. We examine the effects of individual subpackets because, although a chorus rising tone consists of many subpackets, most resonant electrons experience interaction with only one or two subpackets. In the following analysis we identify the wave subpackets most efficient in accelerating seed electrons to MeV energies.

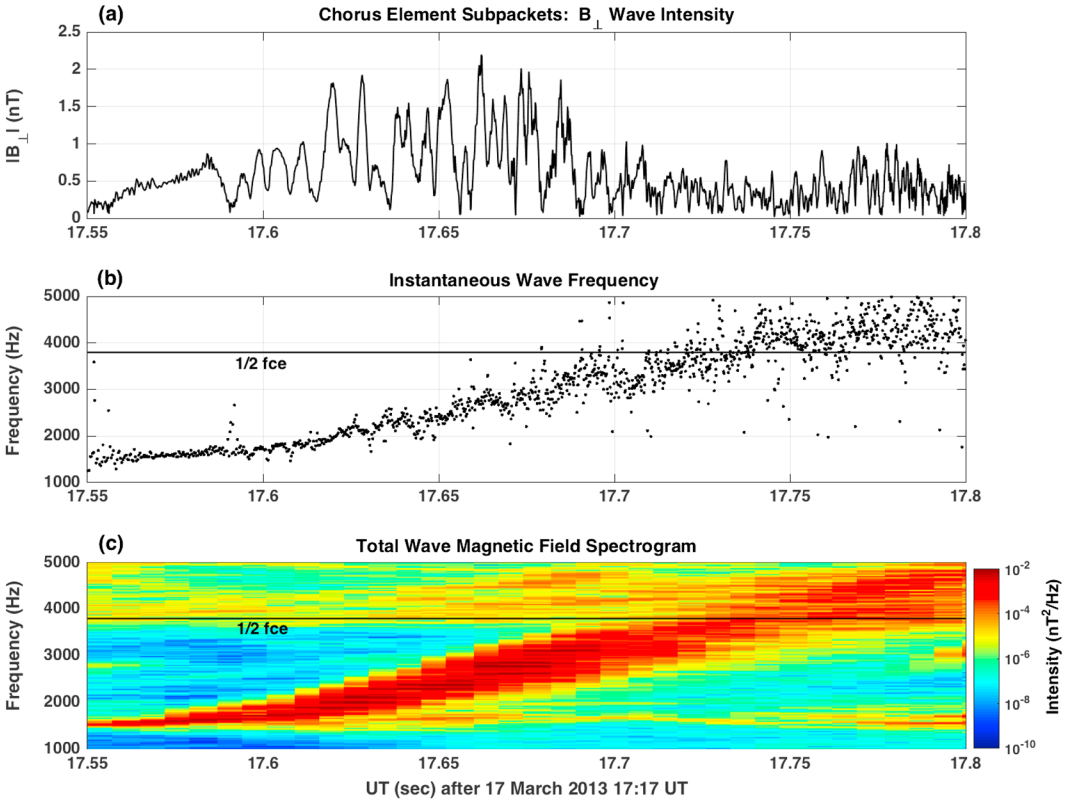

Figure 7. Subpacket analysis of the VLF rising tone shown in Figure 5a is shown. (a) The magnitude of the wave magnetic field in the plane perpendicular to $\mathbf{B_0}$ for individual wave cycles (see text) is shown. Clear modulation of the wave amplitude identifies a sequence of subpackets within the rising tone chorus element, each spanning multiple wave cycles. Each subpacket represents a single cycle of continuous wave growth and damping. (b) Instantaneous wave frequency determined from individual wave cycles is shown. (c) The spectrogram of the total wave magnetic field depicts the growth of the single chorus element over ~250 ms. The black line indicates $\frac{1}{2}f_{ce}$ (~3.8 kHz).

4. Nonlinear Electron Acceleration in VLF Riser Subpackets

To investigate the efficiency of a single chorus element for particle acceleration through cyclotron resonance, we convert the wave perpendicular magnetic field intensity $\mathbf{B}_\perp$ to wave electric field, $\mathbf{E}_\perp$, by multiplying it by the phase velocity, V_p. Following *Omura et al.* [2012], V_p is expressed as a function of the wave angular frequency, ω, the electron cyclotron angular frequency, Ω_e, and the electron plasma angular frequency, ω_{pe}:

$$\xi = \frac{\sqrt{\omega\left(\Omega_e - \omega\right)}}{\omega_{pe}}, \tag{4}$$

$$\chi = \sqrt{\frac{1}{1+\xi^2}}, \tag{5}$$

$$V_p = c\,\chi\,\xi, \tag{6}$$

$$\mathbf{E}_\perp = V_p\,\mathbf{B}_\perp, \tag{7}$$

where c is the speed of light.

Since we know an instantaneous frequency for each half-wave period, we can obtain V_r, V_g, and $V_\perp$ for a specific electron kinetic energy. Here $V_\perp$ is calculated from the electron energy (relativistic γ) and the electron resonance velocity, V_r. We use formulas from equations (13) and (14) in *Omura et al.* [2012] to calculate the group velocity, V_g and the resonance velocity, V_r:

$$V_g = c\,\frac{\xi}{\chi}\left[\xi^2 + \frac{\Omega_e}{2\left(\Omega_e - \omega\right)}\right]^{-1}, \tag{8}$$

$$V_r = c\,\chi\,\xi\left(1-\frac{\Omega_e}{\gamma\,\omega}\right), \tag{9}$$

$$V_\perp = \sqrt{c^2\left(1-\frac{1}{\gamma^2}\right)-V_r^2}, \tag{10}$$

$$k_\perp = \frac{\omega}{V_p}\,\sin\theta, \tag{11}$$

where θ is the wave-normal angle.

The maximum acceleration for an electron in an individual subpacket is

$$\Delta\,E_{\text{cyclotron}}\,(\text{eV}) = \sum\left(0.5\,J_0(\beta)\,\left|\mathbf{E}_\perp\right|\,V_\perp\,V_g\,\delta t\left(\frac{V_g-V_r}{1-(V_g\,V_r)/c^2}\right)^{-1}\right), \tag{12}$$

where δt is a half-wave cycle, and $V_g\,\delta t\left(\frac{V_g-V_r}{1-(V_g\,V_r)/c^2}\right)^{-1}$ gives the interaction time between a resonant electron and a segment of the subpacket corresponding to the half-wave cycle. We take the sum over all wave cycles in the subpacket separately for electrons with a range of initial energies (50 keV to 8 MeV).

In a result similar to that reported by *Santolík et al.* [2014], who applied subpacket analysis to Van Allen Probes observations of chorus waveforms, we find that the wave-normal angle, θ, varies from ~5–20° for the strongest wave subpackets. While the condition $\sin^2\theta \ll 1$ for quasi-parallel propagation is still satisfied, these values indicate that a perpendicular wave number component exists which can change the wave phase substantially for MeV electrons due to their large gyroradii. In particular, with

$$k_\perp = k\sin\theta \sim k\sin 20^\circ \sim 0.34k \quad , \tag{13}$$

then

$$\beta = \gamma\,\frac{V_\perp k_\perp}{\Omega_e} \tag{14}$$

can be of the order of unity. We therefore include a wave amplitude correction factor in equation (12) by multiplying $E_\perp$ by $J_0(\beta)$, where J_0 is a Bessel function of the first kind with index 0.

We also include a 0.5 factor in equation (12) to account for the inhomogeneity factor $-S$ or $\sin\zeta$. (The second-order resonance condition, i.e., the condition for the nonlinear trapping, is given by $\sin\zeta + S = 0$; see equations (56)–(58) of *Nunn and Omura* [2015].) The absolute value of S varies from 0 to 1 depending on the frequency sweep rate and the gradient of the ambient magnetic field. For simplicity, we assume here that the averaged value $-S = 0.5$.

In Figure 8, we show the results of subpacket analysis for the chorus riser at 16:56:30 UT (cf. Figure 5b). Well-developed subpackets at and around $\frac{1}{4}f_{ce}$ are seen, and these result in strong (>100 keV) energy gain for electrons with relativistic initial energies (Figure 8b). Highly coherent instantaneous wave frequencies (Figure 8c) characterize the strongest wave subpackets, and these are also associated with wave-normal angles <20° (Figure 8d). In Figure 9a (black curve) we plot the total possible energy gain (cf. equation (12)) for electrons in cyclotron resonance interactions with the chorus riser of Figure 8 summed over all subpackets. We also plot in red the greatest energy gain for an electron through interactions with a single subpacket. Although not shown, similar results are obtained for the riser shown in Figure 5a.

Cyclotron resonance by relativistic turning acceleration occurs when the electron pitch angle $\text{PA} = \arctan\left(V_\perp/V_r\right) = 90°$, that is, when $V_r = 0$, changing from negative V_r to positive V_r at the reflection point of the electron bounce motion. The blue curve in Figure 9a shows the most probable energy dependence of the RTA acceleration calculated by limiting the energy gain to electrons with $|\text{PA}| > 87°$. For the cases we have analyzed, RTA energy gain curves are sharply peaked around electron initial energies near 1.5 MeV.

In addition to effects from the wave fields perpendicular to $\mathbf{B_0}$, we also find that the chorus elements we have analyzed have a significant parallel component of the wave electric field. Electron acceleration through Landau resonance by the parallel electric field of highly coherent oblique whistler mode waves was first

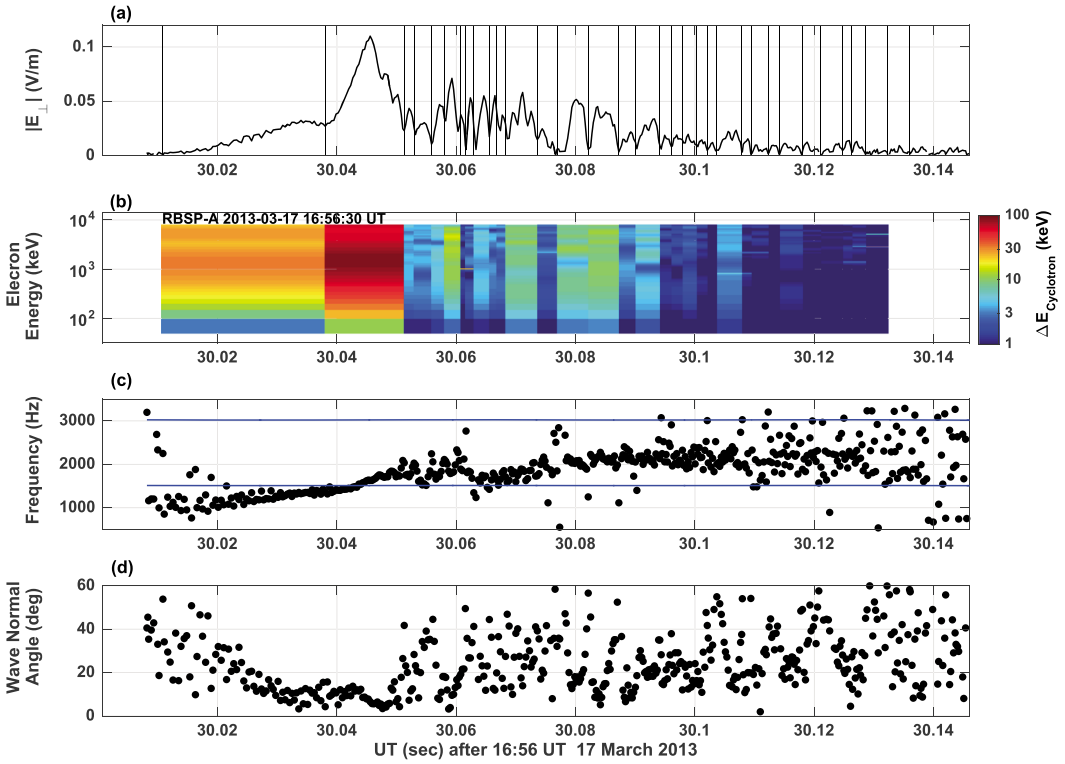

Figure 8. (a) $E_\perp$ subpacket structure is shown for the rising tone shown in Figure 5b. Subpacket boundaries are indicated by vertical lines. Each subpacket represents a single cycle of continuous wave growth and damping and spans a number of wave cycles as determined by zero crossings (see text). (b) Energy gain ($\Delta E_{\text{cyclotron}}$) is shown for electrons in cyclotron interactions calculated by summing across individual subpackets. The results show that MeV seed electrons can be accelerated by >100 keV through interaction with the strongest subpacket. (c) The instantaneous wave frequency calculated at each zero crossing is shown. Highly coherent increasing wave frequencies characterize the strongest subpackets. Horizontal lines indicate $\frac{1}{4}f_{ce}$ and $\frac{1}{2}f_{ce}$. (d) Wave normal angles (5–20°) indicate that the assumption of quasi-parallel propagation is valid for the strongest subpackets.

considered by *Artemyev et al.* [2012], who showed that it could lead to tens of keV acceleration in 100 ms for electrons with 50–100 keV initial energy. Recent Van Allen Probes observations provide evidence for the occurrence of such fast, nonlinear acceleration of radiation belt electrons with energies of 20–100 keV [*Agapitov et al.*, 2015]. To account for this additional source of electron energization, we obtain both the instantaneous frequency from the zero crossings of the $E_\parallel$ wave and the instantaneous wave amplitude $E_\parallel$ from the maximum $E_\parallel$ between zero crossings. We then separately apply subpacket analysis to $E_\parallel$ to calculate the Landau resonance acceleration efficiency for nonlinear trapping in the parallel electric field of the chorus wave, using the expression

$$\Delta E_{\text{Landau}}\,(\text{eV}) = \sum \left(0.5\, J_0(\beta)\, \left|\mathbf{E}_\parallel\right|\, V_p\, V_g\, \delta t \left(\frac{V_g - V_p}{1 - (V_g\, V_p)/c^2} \right)^{-1} \right). \tag{15}$$

Similar to the perpendicular wave calculations, the total and maximum single-subpacket energy gain for electrons in Landau resonance with the parallel component of the wave electric field are shown in Figure 9b. The energy range <200 keV for efficient acceleration by Landau resonance is consistent with previous studies [*Agapitov et al.*, 2015; *Artemyev et al.*, 2015a].

Our analyses of perpendicular and parallel wave effects for the chorus wave elements examined here demonstrate the significant nonlinear acceleration capacity of chorus emissions in the outer radiation belt during substorm injection events. In particular, resonant electrons with initial energies ~1 MeV can gain ~100 keV in a 10–20 ms interaction with a single chorus wave subpacket.

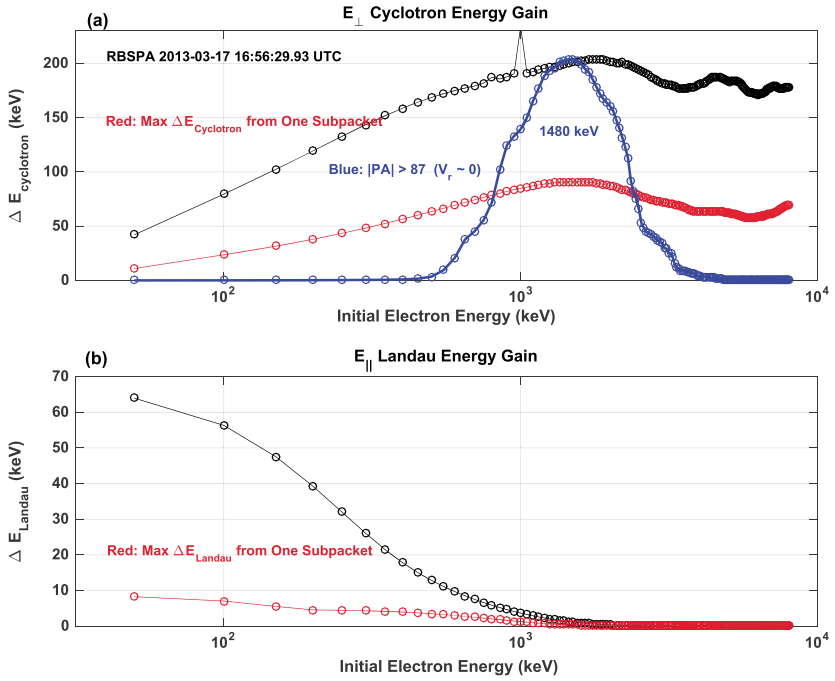

Figure 9. (a) The total energy gain summed over all subpackets for electrons in cyclotron resonance interactions with the chorus riser described in Figure 8 is shown as the black curve. Calculations have been performed separately for electrons with initial energies from 50 keV to 8 MeV. The maximum energy gain for an electron in interactions with a single subpacket is shown in red. For the case under analysis, electrons with initial energies near 1.5 MeV can gain ~100 keV in ~10–20 ms through RTA interaction with the strongest wave packet. The blue curve shows the most probable RTA energy gain considering only electrons with $|PA| > 87°$ (see text). A sharp maximum for electrons with initial energies near 1.5 MeV is found for the cases examined. (b) Total and maximum single subpacket energy gain for electrons in Landau resonance with the parallel component of the observed wave electric field are shown.

5. Supporting Radiation Belt Observations

As shown in Figure 4, dual-satellite Van Allen Probes observations identified the onset of strong (>10X) enhancements for >1 MeV electron flux as a pronounced effect of local acceleration processes during the 17 March 2013 event. Here we examine the consistency of these observations with our theoretical analyses of electron acceleration by chorus rising tones as presented in section 4.

In Figure 10a, we further quantify the observed energy dependence of local acceleration processes by plotting the $L^* = 4.0$ profile of the electron flux ratios shown in Figure 4b. The relative increase in electron flux during the local acceleration event ranges between factors of ~2 and 15 as a function of electron energy and increases exponentially at relativistic electron energies. The combined MagEIS and REPT observations indicate a strong maximum in flux increase (ratio) for electrons with energy near 2 MeV, with a sharp decrease in the observed flux ratios above ~3 MeV. These observations are consistent with the energy dependence associated with the nonlinear energy gain we have calculated in our chorus wave analyses (cf. Figure 9). For the conditions and wave characteristics observed in this event, the cyclotron and Landau resonance mechanisms we have investigated accentuate energy gain at MeV initial electron energies, precisely as seen in the Van Allen Probes electron observations.

To illustrate the effect of nonlinear RTA acceleration on the evolution of the relativistic electron flux spectrum, we have performed a simple calculation in which we iteratively apply the calculated nonlinear energy gain profile (the blue curve in Figure 9a) to the observed initial electron flux profile. We use a 4% trapping probability [e.g., *Artemyev et al.*, 2015a], and electron losses are not taken into account. For each interaction cycle, 4% of the electron flux at each resonant energy is shifted to higher energy according to its calculated nonlinear energy gain where it is added to the 96% of the flux already at that energy. A new flux spectrum is determined, and this process is repeated for each cycle. The evolution of the modeled spectrum is shown in Figure 10b. After 30 cycles, an adequate representation of the observed postacceleration flux spectrum is obtained. A more realistic determination of spectral changes at both low and high energies will need to include particle

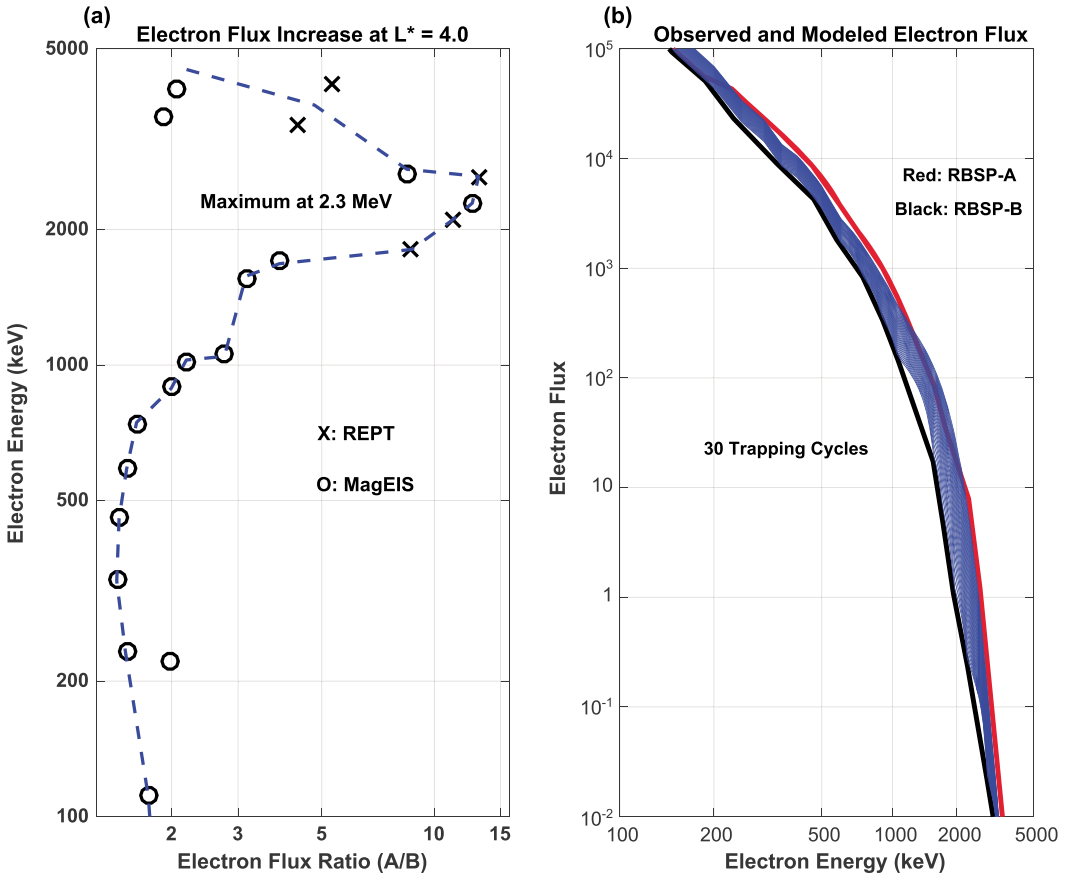

Figure 10. (a) RBSP A/RBSP B electron flux ratios during the 17 March 2013 15:50 UT substorm event at $L^* = 4.0$ are shown across MagEIS and REPT energies (cf. Figure 4b). The relative increase in electron flux during the local acceleration event increases exponentially at relativistic initial electron energies. MagEIS and REPT combined observations indicate a strong maximum for electrons with energies near 2 MeV with a sharp decrease in fluxes above ~3 MeV. (b) Observed electron flux profiles at $L^* = 4$ before (black curve, RBSP B) and after (red curve, RBSP A) the acceleration event are shown along with modeling results (blue curves) indicating the evolution of the initial (black) profile through 30 cycles of nonlinear RTA energy gain (blue curve of Figure 9a) assuming a 4% trapping probability (see text).

losses, the effects of Landau resonances, and energy losses in nontrapped electron populations. We intend to address these issues in subsequent studies.

The ratio of the modeled electron flux profile at $L^* = 4$ after 30 cycles of nonlinear RTA acceleration (cf. Figure 10b) to the observed initial profile is shown in Figure 11a. The nonlinear RTA modeling indicates a 10X flux enhancement confined to low-MeV energies and centered near 2 MeV. For electrons with 0.5 s bounce period, and assuming that strong chorus waves are encountered only 1% of the time, the 30 cycles we have modeled would occur over 1500 s, ~30 min, the approximate characteristic time for the relativistic electron acceleration observed in this event. The observed RBSP A/B electron flux ratios of Figure 10a are replotted in Figure 11b for direct comparison with the theoretical calculations. We conclude that RBSP A/B observations and RTA theoretical predictions show good agreement in identifying the range of electron energies enhanced by local acceleration under the observed conditions.

6. Discussion and Summary

During the local acceleration of radiation belt electrons in interactions with VLF waves, both a source of energy for wave growth and a population of energetic seed electrons are required. Van Allen Probes observations in the core of the outer zone during the recovery phase of the 17 March 2013 storm provide a detailed picture of the role of substorm injections and nonlinear interactions with VLF chorus rising tones in driving local radiation belt acceleration.

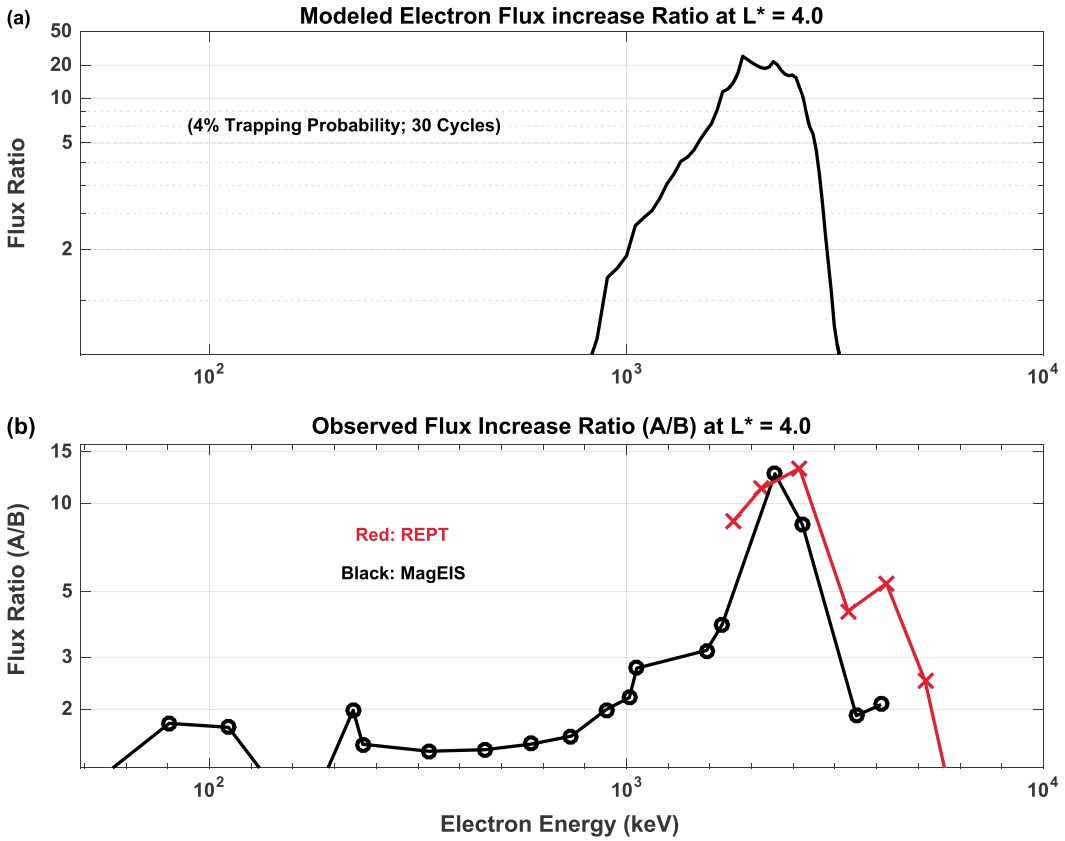

Figure 11. (a) The ratio of the modeled electron flux profile at $L^* = 4$ after 30 cycles of nonlinear RTA acceleration (cf. Figure 10b) to the observed initial profile indicates a 10*x* flux enhancement confined to low-MeV energies and centered near 2 MeV. (b) The observed RBSP A/B electron flux ratios of Figure 10a are replotted for direct comparison with the theoretical calculations. The close agreement between the RBSP A/B observations and RTA theoretical predictions, and the narrow range of MeV energies involved in the prompt RB acceleration, make a strong case for nonlinear processes during this event.

Whenever there are chorus emissions in the radiation belt, a fraction of the resonant seed electrons should be accelerated strongly by the nonlinear processes we have described. Although only a tiny fraction of the radiation belt electrons are affected, the cumulative effect of many chorus emissions must be considered in determining the final characteristics of the radiation belt. MeV electrons circle the Earth due to gradient drift effects in 3–5 min, so the effect of a single chorus emission can have a global impact.

At the same time electromagnetic ion cyclotron rising tone emissions [*Nakamura et al.*, 2014, 2016] can precipitate relativistic electrons very efficiently [*Omura and Zhao*, 2012, 2013]. Both processes take place over similar time scales of a few minutes. In addition, several effects not considered in this paper may interrupt trapping and prevent an optimal nonlinear acceleration. These include amplitude modulation [*Tao et al.*, 2013; *Artemyev et al.*, 2015b] or the presence of additional waves of lower amplitude at different frequencies [*Artemyev et al.*, 2015b].

In this study, subpacket wave analysis has been used to quantify resonant electron energy gain both by relativistic turning acceleration and by ultrarelativistic acceleration through nonlinear trapping by chorus waves. Examining a number of chorus elements at different times and locations during the rapid recovery of the radiation belt during this event, we conclude that electrons with initial energies of hundreds of keV to several MeV can be accelerated by 50 keV–250 keV in resonant interactions with a single VLF rising tone on a time scale of 10–100 ms.

These observations highlight the significant role played by substorm injections in driving local energization and the prompt recovery of the storm-depleted electron radiation belt. The good agreement between theory and observations shown here indicates the efficiency of chorus rising tones for accelerating a seed population

of energetic electrons to MeV energies. We suggest that the rapid acceleration associated with such nonlinear interactions can result in periods of stepwise MeV electron energization on a substorm time scale (~1 h). Sequential injections during the main phase and early recovery phase of a major storm, such as those that occurred on 17–18 March 2013, constitute an important mechanism for the local acceleration of ultrarelativistic electrons and can contribute significantly to the recovery and total energy increase of ≥1 MeV radiation belt electrons as observed during that event.

Acknowledgments
Work at MIT Haystack Observatory was supported by a Van Allen Probes subaward from the University of Minnesota to the Massachusetts Institute of Technology. Work at Kyoto University was supported by MEXT/JSPS KAKENHI grants JP26287120 and JP15H05815. Work at the University of Colorado and the Aerospace Corporation was supported by RBSP-ECT funding provided by JHU/APL contract 967399 under NASA's Prime contract NAS5-01072. We thank the reviewers for helpful comments. All Van Allen Probes data used are available to the public at www.rbsp-ect.lanl.gov.

References

Agapitov, O. V., A. V. Artemyev, D. Mourenas, F. S. Mozer, and V. Krasnoselskikh (2015), Nonlinear local parallel acceleration of electrons through Landau trapping by oblique whistler mode waves in the outer radiation belt, *Geophys. Res. Lett.*, *42*, 10,140–10,149, doi:10.1002/2015GL066887.

Albert, J. M. (2002), Nonlinear interaction of outer zone electrons with VLF waves, *Geophys. Res. Lett.*, *29*(8), 1275, doi:10.1029/2001GL013941.

Artemyev, A. V., V. V. Krasnoselskikh, O. V. Agapitov, D. Mourenas, and G. Rolland (2012), Non-diffusive resonant acceleration of electrons in the radiation belts, *Phys. Plasmas*, *19*(12), 122901, doi:10.1063/1.4769726.

Artemyev, A. V., A. A. Vasiliev, D. Mourenas, A. I. Neishtadt, O. V. Agapitov, and V. Krasnoselskikh (2015a), Probability of relativistic electron trapping by parallel and oblique whistler-mode waves in Earth's radiation belts, *Physics of Plasmas*, *22*(11), 112903, doi:10.1063/1.4935842.

Artemyev, A. V., D. Mourenas, O. V. Agapitov, D. L. Vainchtein, F. S. Mozer, and V. Krasnoselskikh (2015b), Stability of relativistic electron trapping by strong whistler or electromagnetic ion cyclotron waves, *Physics of Plasmas*, *22*(8), 82901, doi:10.1063/1.4927774.

Baker, D. N., et al. (2013a), The Relativistic Electron-Proton Telescope (REPT) instrument on board the Radiation Belt Storm Probes (RBSP) spacecraft: Characterization of Earth's radiation belt high-energy particle populations, *Space Sci. Rev.*, *179*(1–4), 337–381, doi:10.1007/s11214-012-9950-9.

Baker, D. N., et al. (2013b), A long-lived relativistic electron storage ring embedded in Earth's outer Van Allen belt, *Science*, *340*(6129), 186–190, doi:10.1126/science.1233518.

Baker, D. N., et al. (2014), Gradual diffusion and punctuated phase space density enhancements of highly relativistic electrons: Van Allen Probes observations, *Geophys. Res. Lett.*, *41*(5), 1351–1358, doi:10.1002/2013GL058942.

Blake, J. B., et al. (2013), The Magnetic Electron Ion Spectrometer (MagEIS) instruments aboard the Radiation Belt Storm Probes (RBSP) spacecraft, *Space Sci. Rev.*, *179*(1–4), 383–421, doi:10.1007/s11214-013-9991-8.

Bortnik, J., R. M. Thorne, and U. S. Inan (2008), Nonlinear interaction of energetic electrons with large amplitude chorus, *Geophys. Res. Lett.*, *35*(21), L21102, doi:10.1029/2008GL035500.

Boyd, A. J., et al. (2014), Quantifying the radiation belt seed population in the 17 March 2013 electron acceleration event, *Geophys. Res. Lett.*, *41*, 2275–2281, doi:10.1002/2014GL059626.

Brautigam, D. H., and J. M. Albert (2000), Radial diffusion analysis of outer radiation belt electrons during the October 9, 1990, magnetic storm, *J. Geophys. Res.*, *105*(A1), 291–309, doi:10.1029/1999JA900344.

Cattell, C., et al. (2008), Discovery of very large amplitude whistler-mode waves in Earth's radiation belts, *Geophys. Res. Lett.*, *35*, L01105, doi:10.1029/2007GL032009.

Foster, J. C., and T. J. Rosenberg (1976), Electron precipitation and VLF emissions associated with cyclotron resonance interactions near the plasmapause, *J. Geophys. Res.*, *81*(13), 2183–2192, doi:10.1029/JA081i013p02183.

Foster, J. C., et al. (2014), Prompt energization of relativistic and highly relativistic electrons during a substorm interval: Van Allen Probes observations, *Geophys. Res. Lett.*, *41*, 20–25, doi:10.1002/2013GL058438.

Hikishima, M., et al. (2009), Full particle simulation of whistler mode rising chorus emissions in the magnetosphere, *J. Geophys. Res.*, *114*, A01203, doi:10.1029/2008JA013625.

Horne, R. B., et al. (2005), Timescale for radiation belt electron acceleration by whistler mode chorus waves, *J. Geophys. Res.*, *110*, A03225, doi:10.1029/2004JA010811.

Jaynes, A. N., et al. (2015), Source and seed populations for relativistic electrons: Their roles in radiation belt changes, *J. Geophys. Res. Space Physics*, *120*, 7240–7254, doi:10.1002/2015JA021234.

Katoh, Y., and Y. Omura (2007), Relativistic particle acceleration in the process of whistler mode chorus wave generation, *Geophys. Res. Lett.*, *34*, L13102, doi:10.1029/2007GL029758.

Kletzing, C. A., et al. (2013), The Electric and Magnetic Field Instrument Suite and Integrated Science (EMFISIS) on RBSP, in *The Van Allen Probes Mission*, pp. 127–181, Springer, Boston, Mass., doi:10.1007/978-1-4899-7433-4_5.

Li, W., et al. (2014), Radiation belt electron acceleration by chorus waves during the 17 March 2013 storm, *J. Geophys. Res. Space Physics*, *119*, 4681–4693, doi:10.1002/2014JA019945.

Mauk, B. H., et al. (2013), Science objectives and rationale for the radiation belt storm probes mission, *Space Sci. Rev.*, *179*(1–4), 3–27, doi:10.1007/s11214-012-9908-y.

Miyoshi, Y., A. Morioka, H. Misawa, T. Obara, T. Nagai, and Y. Kasahara (2003), Rebuilding process of the outer radiation belt during the 3 November 1993 magnetic storm: NOAA and Exos-D observations, *J. Geophys. Res.*, *108*(A1), 1004, doi:10.1029/2001JA007542.

Miyoshi, Y., R. Kataoka, Y. Kasahara, A. Kumamoto, T. Nagai, and M. F. Thomsen (2013), High-speed solar wind with southward interplanetary magnetic field causes relativistic electron flux enhancement of the outer radiation belt via enhanced condition of whistler waves, *Geophys. Res. Lett.*, *40*, 4520–4525, doi:10.1002/grl.50916.

Nakamura, S., Y. Omura, and V. Angelopoulos (2016), A statistical study of EMIC rising and falling tone emissions observed by THEMIS, *J. Geophys. Res. Space Physics*, *121*, 8374–8391, doi:10.1002/2016JA022353.

Nakamura, S., et al. (2014), Electromagnetic ion cyclotron rising tone emissions observed by THEMIS probes outside the plasmapause, *J. Geophys. Res. Space Physics*, *119*, 1874–1886, doi:10.1002/2013JA019146.

Nunn, D., and Y. Omura (2015), A computational and theoretical investigation of nonlinear wave-particle interactions in oblique whistlers, *J. Geophys. Res. Space Physics*, *120*, 2890–2911, doi:10.1002/2014JA020898.

Omura, Y., and D. Nunn (2011), Triggering process of whistler mode chorus emissions in the magnetosphere, *J. Geophys. Res.*, *116*, A05205, doi:10.1029/2010JA016280.

Omura, Y., and Q. Zhao (2012), Nonlinear pitch angle scattering of relativistic electrons by EMIC waves in the inner magnetosphere, *J. Geophys. Res.*, *117*, A08227, doi:10.1029/2012JA017943.

Omura, Y., and Q. Zhao (2013), Relativistic electron microbursts due to nonlinear pitch angle scattering by EMIC triggered emissions, *J. Geophys. Res. Space Physics*, *118*, 5008–5020, doi:10.1002/jgra.50477.

Omura, Y., N. Furuya, and D. Summers (2007), Relativistic turning acceleration of resonant electrons by coherent whistler mode waves in a dipole magnetic field, *J. Geophys. Res.*, *112*, A06236, doi:10.1029/2006JA012243.

Omura, Y., Y. Katoh, and D. Summers (2008), Theory and simulation of the generation of whistler-mode chorus, *J. Geophys. Res.*, *113*, A04223, doi:10.1029/2007JA012622.

Omura, Y., D. Nunn, and D. Summers (2012), Generation processes of whistler mode chorus emissions: Current status of nonlinear wave growth theory, in *Dynamics of the Earth's Radiation Belts and Inner Magnetosphere, Geophys. Monogr. Ser.*, vol. 199, edited by D. Summers et al., pp. 243–254, AGU, Washington, D. C., doi:10.1029/2012GM001347.

Omura, Y., et al. (2009), Nonlinear mechanisms of lower-band and upper-band VLF chorus emissions in the magnetosphere, *J. Geophys. Res.*, *114*, A07217, doi:10.1029/2009JA014206.

Omura, Y., et al. (2015), Formation process of relativistic electron flux through interaction with chorus emissions in the Earth's inner magnetosphere, *J. Geophys. Res. Space Physics*, *120*, 9545–9562, doi:10.1002/2015JA021563.

Reeves, G. D., et al. (2013), Electron acceleration in the heart of the Van Allen radiation belts, *Science*, *341*(6149), 991–994, doi:10.1126/science.1237743.

Roederer, J. G., and H. Zhang (2014), Dynamics of magnetically trapped particles, in *Astrophysics and Space Science Library*, vol. 403, Springer, Berlin., doi: 10.1007/978-3-642-41530-2.

Santolík, O., D. A. Gurnett, J. S. Pickett, M. Parrot, and N. Cornilleau-Wehrlin (2003), Spatio-temporal structure of storm-time chorus, *J. Geophys. Res.*, *108*(A7), 1278, doi:10.1029/2002JA009791.

Santolík, O., D. A. Gurnett, J. S. Pickett, M. Parrot, and N. Cornilleau-Wehrlin (2004), A microscopic and nanoscopic view of storm time chorus on 31 March 2001, *Geophys. Res. Lett.*, *31*, L02801, doi:10.1029/2003GL018757.

Santolík, O., C. A. Kletzing, W. S. Kurth, G. B. Hospodarsky, and S. R. Bounds (2014), Fine structure of large-amplitude chorus wave packets, *Geophys. Res. Lett.*, *41*, 293–299, doi:10.1002/2013GL058889.

Sugiyama, H., et al. (2015), Electromagnetic ion cyclotron waves in the Earth's magnetosphere with a kappa-Maxwellian particle distribution, *J. Geophys. Res. Space Physics*, *120*, 8426–8439, doi:10.1002/2015JA021346.

Summers, D., and Y. Omura (2007), Ultra-relativistic acceleration of electrons in planetary magnetospheres, *Geophys. Res. Lett.*, *34*, L24205, doi:10.1029/2007GL032226.

Summers, D., R. M. Thorne, and F. Xiao (1998), Relativistic theory of wave-particle resonant diffusion with application to electron acceleration in the magnetosphere, *J. Geophys. Res.*, *103*(A9), 20,487–20,500, doi:10.1029/98JA01740.

Tao, X., J. Bortnik, J. Albert, R. Thorne, and W. Li (2013), The importance of amplitude modulation in nonlinear interactions between electrons and large amplitude whistler waves, *J. Atmos. Sol. Terr. Phys.*, *99*, 67–72, doi:10.1016/j.jastp.2012.05.012.

Thorne, R. M., et al. (2013), Rapid local acceleration of relativistic radiation-belt electrons by magnetospheric chorus, *Nature*, *504*(7480), 411–414, doi:10.1038/nature12889.

Tsyganenko, N. A., and M. I. Sitnov (2005), Modeling the dynamics of the inner magnetosphere during strong geomagnetic storms, *J. Geophys. Res.*, *110*, A03208, doi:10.1029/2004JA010798.

Ukhorskiy, A. Y., et al. (2014), Enhanced radial transport and energization of radiation belt electrons due to drift orbit bifurcations, *J. Geophys. Res. Space Physics*, *119*, 163–170, doi:10.1002/2013JA019315.

Ukhorskiy, A. Y., et al. (2015), Global storm time depletion of the outer electron belt, *J. Geophys. Res. Space Physics*, *120*, 2543–2556, doi:10.1002/2014JA020645.

Wygant, J. R., et al. (2013), The electric field and waves instruments on the Radiation Belt Storm Probes Mission, *Space Sci. Rev.*, *179*(1–4), 183–220, doi:10.1007/s11214-013-0013-7.

Xiao, F., et al. (2014), Chorus acceleration of radiation belt relativistic electrons during March 2013 geomagnetic storm, *J. Geophys. Res. Space Physics*, *119*, 3325–3332, doi:10.1002/2014JA019822.